DOI:10.1093/jnci/djt212
Advance Access publication September 19, 2013

ARTICLE

Role of Type II Pneumocyte Senescence in Radiation-Induced Lung Fibrosis

Deborah E. Citrin, Uma Shankavaram, Jason A. Horton, William Shield III, Shuping Zhao, Hiroaki Asano, Ayla White, Anastasia Sowers, Angela Thetford, and Eun Joo Chung

Manuscript received May 1, 2013; revised June 21, 2013; accepted June 24, 2013.

Correspondence to: Deborah Citrin, MD, Radiation Oncology Branch, National Cancer Institute, Bldg 10 CRC, B2-3500, Bethesda, MD (e-mail: citrind@mail.nih.gov).

Background Radiation is a commonly delivered therapeutic modality for cancer. The causes underlying the chronic, progressive nature of radiation injury in the lung are poorly understood.

Methods C57Bl/6NCr mice were exposed to thoracic irradiation (n = 3 per dose and time point for tissue collection). Microarray analysis of gene expression from irradiated murine lung was performed using one-way analysis of variance with post hoc Scheffe analysis. Senescence and type II airway epithelial cell (AECII) count were assayed in irradiated murine lung tissue (n = 3 per condition). Irradiated mice were treated with diphenyleneiodonium (DPI), an inhibitor of NADPH oxidase (NOX), and fibrosis was assessed by collagen assays. All statistical tests were two-tailed.

Results Gene expression in lung tissue from mice irradiated to 17.5 Gy clustered with that of aged unirradiated mice. Only fibrogenic exposures led to AECII senescence (0 Gy: 0.66% +/– 0.67%; 5 Gy: 4.5% +/– 1.19%; 17.5 Gy: 18.7% +/– 3.05; $P = .007$) and depletion (0 Gy: 2.89 per alveolus +/– 0.26; 5 Gy: 2.41 +/– 0.19; 17.5 Gy: 1.6 +/– 0.14; $P < .001$) at 30 weeks. Treatment of irradiated mice with DPI for 16 weeks markedly reduced collagen accumulation (5×6 Gy: 57.26 μg/lung +/– 9.91; 5×6 Gy +/– DPI: 36.54μg/lung +/– 4.39; $P = .03$) and AECII senescence (5×6 Gy: 37.61% +/– 4.82%; 5×6 Gy +/– DPI: 12.38% +/– 2.78; $P < .001$).

Conclusions These studies identify senescence as an important process in AECII in vivo and indicate that NOX is a critical mediator of radiation-induced AECII senescence and pulmonary fibrosis.

J Natl Cancer Inst;2013;105:1474–1484

Two-thirds of cancer patients receive radiotherapy. Pulmonary fibrosis may develop after thoracic irradiation, with symptoms ranging from mild dyspnea to chronic pulmonary insufficiency (1). The etiology of radiation-induced pulmonary fibrosis (RIPF) is incompletely understood, and effective interventions are lacking.

Pneumocytes play a critical role in lung homeostasis. Type II pneumocytes (airway epithelial cell type II [AECII]) produce surfactant and repopulate type I and II pneumocytes after insult (2,3). Extensive AECII loss stimulates macrophage influx and proinflammatory cytokine elaboration, with resulting fibrosis (4,5). Surviving injured pneumocytes undergo epithelial–mesenchymal transition and elaborate transforming growth factor β (6,7).

Although pneumocyte apoptosis after irradiation has been described, the role of processes that limit replicative reserve are largely unexplored (8,9). Senescence occurs in tumor cells as a response to radiation and correlates with reduced clonogenic survival (10–12). Senescent cells secrete proinflammatory cytokines, such as interleukin 6, transforming growth factor β, and interleukin 1-α, which are implicated in RIPF (13,14). We sought to further understand RIPF using microarray as a discovery platform.

Methods

Mice and Irradiation

Mouse studies were institutionally approved and in accordance with the guidelines of the Institute of Laboratory Animal Resources, National Research Council. Ten-week-old female C57BL/6NCr mice (Frederick National Laboratory, Frederick, MD) were restrained for irradiation of the thorax with lead shielding the remainder of the body. Radiation was delivered with an X-RAD 320 (Precision X-Ray, North Branford, CT) with 2.0-mm Al filtration (300 kv peak) at 2.61 Gy/minute.

Mice were treated to 0 Gy (control), 5 Gy, 17.5 Gy, 5×5 Gy, or 5×6 Gy (n = 20 per dose) and followed for survival through 30 weeks. Additional cohorts were treated for intermediate time-point tissue collection. Lethality of 5×6 Gy prevented collection at 30 weeks. Inflated lung tissue was embedded in optimal cutting temperature compound (VWR, West Chester, PA), formalin fixed and paraffin embedded, or snap frozen and stored at –80°C until use.

Separate cohorts (n = 8 mice per group) were treated with diphenyleneiodonium (DPI, Sigma, St. Louis, MO) 1 mg/kg in phosphate buffered saline or vehicle, delivered by subcutaneous

injection beginning immediately after irradiation (5×6 Gy) and continuing 5 days per week for 16 weeks.

Microarray and Statistical Methods

RNA from total lung of mice exposed to 0 Gy, 5 Gy, or 17.5 Gy at 2, 4, 8, 16, and 30 weeks after irradiation (n = 3 per condition) was extracted in TRIZol (Invitrogen, Carlsbad, CA) and purified with RNAeasy Plus kits (Qiagen, Valencia, CA). Biotin-labeled antisense cRNA was generated using the One-Cycle Target Labeling kit (Affymetrix, Santa Clara, CA). Labeled cRNA was chemically fragmented and hybridized to Mouse Genome 430 2.0 GeneChips (Affymetrix). Hybridized chips were scanned with a GeneChip scanner 3000 7G. These data were deposited in NCBI's Gene Expression Omnibus (15), accession number GSE41789.

Statistical analyses of microarray data were performed with R/Bioconductor (http://www.bioconductor.org) (16). Datasets were normalized using the robust multichip average algorithm. Intensity values were log2 transformed, probe sets were mapped to official gene symbols, and *Z* score transformation was used. A filter with standard deviation of 1.5 was implemented to remove invariant genes. To estimate differences between doses across all time points, a one-way analysis of variance (ANOVA) with post hoc Scheffe analysis was used. Paired comparisons were estimated by Tukey honest significant difference method, applied to the fitted ANOVA model. Genes changed ($P \leq .05$) between control, 5 Gy, and 17.5 Gy were considered for further analysis. Paired comparisons were performed with each dose within each time point.

Senescence Gene Enrichment

A detailed description of senescence gene enrichment is included in the Supplementary Methods (available online). Briefly, a senescence and aging gene set was developed by combining a previously reported DNA damage-associated senescence (DASS) signature (17), a modified secretory senescence signature (mSS) (17), and tissue-specific aging genes from the AGEMAP database (18). To identify genes that showed an association ($P \leq .05$) with the senescence signature, an enrichment analysis was performed using Fisher exact test. For time point–specific comparisons, each gene was scored depending on whether the expression of that gene was in a pro-senescent direction (relative to control), as previously described (17).

Histology, Tissue Staining, and Collagen Assays

Fibrosis was assessed by Masson trichrome technique (Sigma-Aldrich, St. Louis, MO). For immunohistochemistry (described in the Supplementary Methods, available online), deparaffinized sections were subjected to antigen retrieval, blocking, and primary antibody incubation. Antibodies against pro-surfactant C, p21, and NOX4 were obtained from Abcam (Cambridge, MA), and an antibody against 8-OHdG was obtained from Genox (Baltimore, MD). Immunoreactivity was visualized by ImmPRESS/ImmPACT histochemistry (Vector Laboratories, Burlingame, CA) with nuclear fast red counterstaining.

Senescence-associated β-galactosidase (β-gal) activity was assessed with a commercially available assay (Abcam, Cambridge, MA). Frozen sections were incubated with 10 μM dihydroethidium (DHE; Life Technologies, Grand Island, NY) in a light-protected humidified chamber at 37°C for 30 minutes. To visualize apoptosis, terminal deoxynucleotidyl transferase deoxynucleotidyl transferase (dUTP) nick end labeling (TUNEL) was performed (ApopTag, Millipore, Bilerica, MA). The number of senescent, DHE-positive, or TUNEL-positive cells was counted on five 20× fields per mouse and expressed as a percentage of total AECII.

Lung collagen content was assessed with the sircol and hydroxyproline assays, as described in the Supplementary Methods (available online).

In Vitro Studies

Primary pneumocytes were isolated from C57BL/6NCr mice as detailed in the Supplementary Methods (available online). Enriched pneumocytes were treated with DPI (Sigma) or catalase (Sigma) 1 hour before irradiation. Superoxide production was visualized after incubation with 10 μM DHE for 30 minutes. For immunocytochemistry, primary immunoreactivity was detected with fluorophore-conjugated secondary antibodies (Life Technologies, Grand Island, NY). Coculture experiments with NIH-3T3 and pneumocytes are described in the Supplementary Methods (available online).

Statistical Analysis

Survival was estimated with the Kaplan–Meier method and unstratified log-rank statistical analysis to test for differences, with pairwise comparison between groups. For mechanistic studies, comparisons between conditions were evaluated with ANOVA with Bonferroni correction. A *P* value of less than .05 was considered statistically significant. All statistical tests were two-sided. Tissue experiments were conducted in triplicate. In vitro studies were validated in duplicate experiments.

Results

Fibrosis Model

Mice treated to 0 Gy or 5 Gy uniformly survived through 30 weeks, whereas fibrogenic irradiation reduced survival (log rank $P < .001$). Three mice in the 17.5 Gy arm and two mice in the 5×6 Gy arm were censored from analysis (all between 3 and 7 weeks) because of severe dermatitis. The median survival was 24.4 weeks for 17.5 Gy (95% confidence interval [CI] = 22.3 to undefined), 25.4 weeks for 5×5 Gy (95% CI = 23.4 to undefined), and 17.6 weeks for 5×6 Gy (95% CI = 17.6 to 19.6) (Figure 1A; Supplementary Table 1, available online). Mice exposed to fibrogenic doses developed coat graying in the irradiated region (Figure 1B). Extensive fibrosis was evident in the lungs of C57BL6/NCr mice at 20 weeks after 5×6 Gy and 30 weeks after 17.5 Gy and 5×5 Gy. No histologic differences were evident between control and 5 Gy lungs at 30 weeks (Figure 1C).

Effects of Radiation on Gene Expression

Microarray analysis was used to examine gene expression in lung (control, 5 Gy, 17.5 Gy) at 2, 4, 8, 16, and 30 weeks after irradiation. Of the 20 458 mouse genes screened, 662 genes were differentially expressed for the comparison of control with 5 Gy, 822 for the comparison of control with 17.5 Gy, and 900 for the comparison of 5 Gy with 17.5 Gy (Figure 2A).

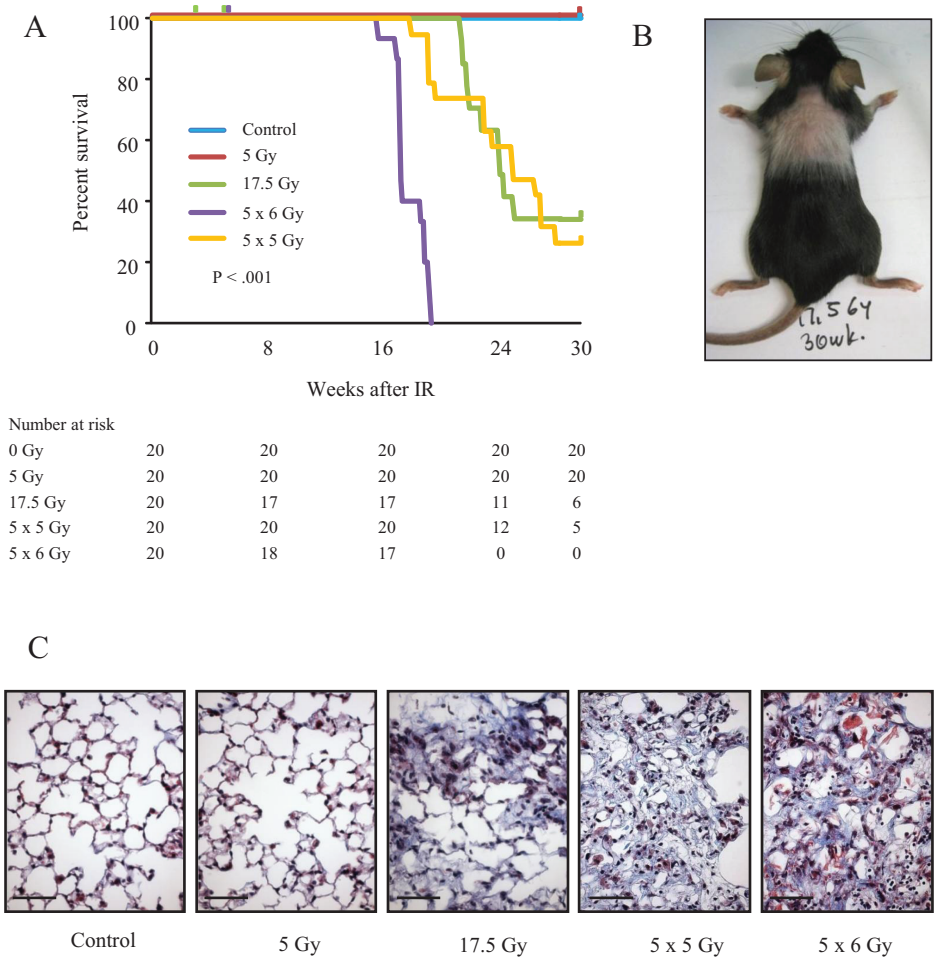

Number at risk					
0 Gy	20	20	20	20	20
5 Gy	20	20	20	20	20
17.5 Gy	20	17	17	11	6
5 x 5 Gy	20	20	20	12	5
5 x 6 Gy	20	18	17	0	0

Figure 1. Fibrotic lung injury models. C57Bl/6NCr mice were exposed to 0 Gy (control), 5 Gy, 17.5 Gy, 5×6 Gy, or 5×5 Gy of thoracic irradiation (IR). **A**) Kaplan–Meier plot of survival of irradiated mice through 30 weeks. The reported *P* value is from log rank comparing survival curves. All statistical tests were two-sided. The number at risk for each time point is listed in the table directly below the survival curve. **B**) Image of a mouse treated with 17.5 Gy at 30 weeks. The coat in the treated region thins and lightens. **C**) Masson trichrome staining of lung tissue collected at 30 weeks after IR (control, 5 Gy, 17.5 Gy, 5×5 Gy) or 20 weeks after IR (5×6 Gy). Lungs treated to 17.5 Gy or with the fractionated doses develop foci of fibrosis. Collagen: **blue**; nuclei: **purple**; cytoplasm/epithelia: **pink**. Scale bar = 40 μm.

Unsupervised hierarchical clustering of the samples resulted in three subdivisions (Figure 2B). The first cluster included 17.5 Gy specimens and the oldest control specimens (week 30), suggesting that expression data for the 17.5 Gy samples were more closely related to the 30-week-old control samples. The second cluster branched into two subclusters: one included specimens treated with 5 Gy and intermediate aged controls (week 16), and a second contained young controls (weeks 2–8).

Based on the clustering of 17.5 Gy–treated lung with aged mice, we evaluated the expression of three published gene signatures of cellular senescence (17) and aging (18). Initially, we compared genes changed after radiation (17.5 Gy + 5 Gy vs control) across time points. Gene expression across the samples was altered, predominantly in the AGEMAP lung (odds ratio [OR] = 2.03; 95% CI = 1.11 to 3.77; *P* = .02), DASS (OR = 6.09; 95% CI = 1.22 to 58.81; *P* = .02), and mSS gene sets (OR = 4.57; 95% CI = 1.14 to 26.25; *P* = .02) (Table 1). By combining the DASS, mSS, and AGEMAP lung gene sets, a variation in expression across treatments was seen (OR = 2.6; 95% CI = 1.6 to 4.47; *P* < .001). To incorporate the direction of the differential expression, a comparison was performed in which gene expression was analyzed by dose and time (Supplementary Table 2, available online). This analysis confirmed the association of senescence signature genes in 17.5 Gy samples ($P \leq .05$ for all comparisons of DASS + mSS + Lung), but not in 5 Gy samples.

Expression data were again subjected to hierarchical clustering using the 45 genes from AGEMAP (lung), mSS, and DASS that were differentially expressed (Figure 3A). This analysis resulted in two major clusters. One cluster included young mice receiving 5 Gy and young unirradiated mice, as well as the youngest (week 2) 17.5 Gy–treated mice. A second cluster included mice receiving 17.5 Gy (4 weeks and later) and older mice (control and 5 Gy).

Effects of Irradiation on AECII Senescence

Clustering of older control mice with 17.5 Gy led us to hypothesize that fibrogenic radiation results in cellular senescence. Indeed, the number of senescent cells in murine lung was increased as early as 4 weeks after exposure to 17.5 Gy compared with mice exposed to 5 Gy or no irradiation (0 Gy: 2.4 per low power field +/- 1.67 [standard deviation, SD]; 5 Gy: 5.2 +/- 2.17; 17.5 Gy: 18.4 +/- 7.3;

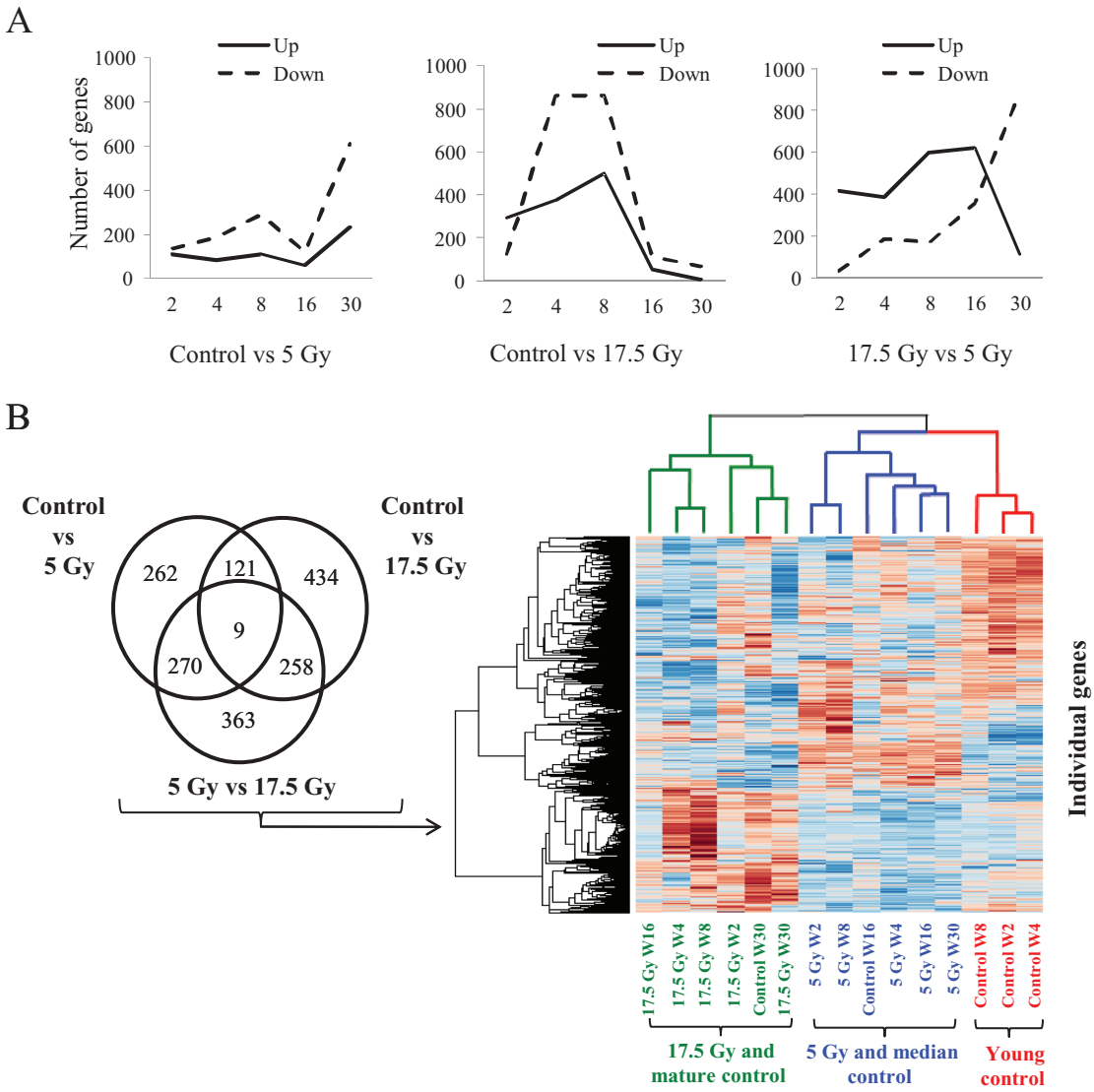

Figure 2. Effects of irradiation (IR) on gene expression in lung tissue. C57Bl/6NCr mice were exposed to 0 Gy (control), 5 Gy, or 17.5 Gy thoracic IR. Samples of lung tissue (n = 3 per dose and time point) were collected at intervals after IR and in control mice for microarray analysis. **A**) Pattern of differentially expressed genes ($P < .05$ by analysis of variance with post hoc Scheffe analysis) in lung tissue by microarray analysis by treatment comparison over time. All statistical tests were two-sided. **B**) Unsupervised hierarchical clustering of differentially expressed genes in lung between treatments. Lung treated with 17.5 Gy clusters with aged unirradiated specimens (**green** color coding of dendrogram and samples), lung treated to 5 Gy clustered with intermediate aged controls (**blue**), and young controls grouped separately (**red**). W = week.

$P < .001$) (Figure 3B). Senescent cells costained for p21 and surfactant associated protein C (pro-SPC), a marker of AECIIs (Figure 3C).

Apoptosis is a reported mechanism of pneumocyte death after irradiation (8,19). To determine the relative importance of apoptosis and senescence in AECII after irradiation, TUNEL and β-gal/p21 staining was performed in combination with immunohistochemistry for pro-SPC in lung tissue. Apoptosis peaked at 2 weeks but occurred to a similar extent after exposure to nonfibrogenic and fibrogenic doses ($P = .41$ by ANOVA for comparison of all radiation doses) (Figure 4A). In contrast, senescence was increased in a time- and dose-dependent fashion after fibrogenic irradiation, with rates of AECII senescence at 30 weeks of 0.66% +/- 0.67% (SD), 4.5% +/- 1.19%, and 18.7% +/- 3.05% for 0 Gy, 5 Gy, and 17.5 Gy respectively ($P = .007$) (Figure 4B).

The abundance of AECII was evaluated as a surrogate of lung regenerative capacity. Despite similar levels of early apoptosis in all irradiated mice, AECII counts recovered only in mice receiving 5 Gy (Figure 4C), whereas they remained depressed at 30 weeks after fibrogenic irradiation (0 Gy: 2.89 AECII per alveolus +/- 0.26 [SD], 5 Gy: 2.41 +/- 0.19, and 17.5 Gy: 1.6 +/- 0.14; $P < .001$). Collectively, these data support that senescence contributes to AECII depletion after fibrogenic irradiation.

Role of NOX in AECII Senescence

Oxidative stress, a consequence of irradiation, is implicated in nonreplicative cellular senescence (20–23). Superoxide generation was evaluated with DHE. The number of cells oxidizing DHE increased at week 2 in irradiated lungs (0 Gy: 1.85% +/- 0.16% [SD]; 17.5 Gy: 14.20% +/- 1.58%; $P < .001$) (Figure 5A; Supplementary Figure 1, available online) and was elevated in fibrogenic doses compared with 5 Gy (5 Gy: 8.00% +/- 0.32% [SD]; 17.5 Gy: 14.20% +/- 1.58%; $P < .001$).

Table 1. Senescence and aging genes in irradiated lung*

Gene signature	Genes in category	DE, No.	EF	OR (95% CI)	*P*
AGEMAP adrenal	10	6	1.51	2.28 (0.54 to 11.01)	.21
AGEMAP cerebellum†	13	5	1.05	1.09 (0.27 to 3.98)	1.00
AGEMAP eye†	159	65	1.13	1.24 (0.88 to 1.74)	.20
AGEMAP gonads†	31	10	1.10	1.01 (0.41 to 2.42)	1.00
AGEMAP heart†	9	3	0.84	0.76 (0.12 to 3.56)	1.00
AGEMAP spinal cord†	37	20	1.40	1.91 (0.94 to 3.93)	.06
AGEMAP spleen†	18	5	0.79	0.69 (0.19 to 2.16)	.61
AGEMAP thymus†	183	82	1.14	1.25 (0.92 to 1.7)	.15
AGEMAP lung†	52	28	1.44	2.03 (1.11 to 3.77)	.02
DASS‡	12	8	2.02	6.09 (1.22 to 58.81)	.02
mSS‡	16	9	1.89	4.57 (1.14 to 26.25)	.02
DASS + mSS	28	17	1.95	5.18 (1.83 to 17.98)	<.001
DASS + mSS + lung	77	45	1.60	2.65 (1.60 to 4.47)	<.001

* *P* values were calculated by Fisher exact test for the comparison between treatments. All statistical tests were two-sided. CI = confidence interval; DASS = DNA damage-associated senescence; DE = number of genes from each signature or category with differential expression ($P < .05$) across treatments in the array dataset; EF = enrichment factor, a parameter that estimates the extent to which genes identified in the published gene categories are overrepresented in the pool of genes ($P < .05$) that show changes in expression in the microarray data; mSS = modified secretory senescence signature; OR = odds ratio, odds of enrichment of the specified gene set or category within the pool of genes ($P < .05$) that show changes in expression in the microarray data versus all genes in the array dataset.

† Genes from the AGEMAP database (5) evaluated in the microarray dataset.

‡ DASS and mSS signatures (6) evaluated in the microarray dataset.

To determine if AECII senescence in irradiated lung resulted from an intrinsic effect, primary murine pneumocytes were irradiated with 5 Gy and 17.5 Gy. As observed in the lung, pneumocyte cultures exposed to 17.5 Gy exhibited increased prevalence of DHE oxidation (0 Gy: 2.86% +/- 0.64% [SD], 17.5 Gy: 47.95% +/- 7.43%; $P < .001$) and senescence (0 Gy: 9.5% +/- 6.36% [SD]; 17.5 Gy: 40.05% +/- 1.41%; $P = .02$), (Figure 5, B and C). Costaining confirmed that the majority of senescent pneumocytes exposed to 17.5 Gy also oxidized DHE (97.50%; SD = 1.6%) (Figure 5D).

Oxidant stress may result in senescence, but senescence may also stimulate free-radical generation (24). We hypothesized that NOX-dependent oxidative stress after irradiation induced AECII senescence. Inhibition of NOX with DPI ablated DHE oxidation (17.5 Gy: 47.95% +/- 7.43% [SD]; 17.5 Gy + DPI: 1.19% +/- 1.68%; $P = .008$) and senescence (17.5 Gy: 40.05% +/- 1.41% [SD]; 17.5 Gy + DPI: 0.00 [none detected]; $P = 0.01$; 95% CI = 22.76 to 57.24) in irradiated primary pneumocytes (Figure 5C). Furthermore, DPI treatment of primary pneumocytes prevented p21 expression and 8OHdG adduct accumulation after 17.5 Gy, whereas catalase treatment had no effect on these endpoints (Supplementary Figures 3 and 4, available online).

Paracrine Effects of Senescent Pneumocytes

To determine whether senescent pneumocytes initiate fibrotic processes or are merely a marker of injury, we cocultured irradiated AECII with unirradiated AECII or fibroblasts. Coculture with 17.5 Gy irradiated pneumocytes was sufficient to induce senescence in unirradiated pneumocytes from C57BL6/30ShaJ-UBCtgGFP mice (Figure 5, E and F), an effect not observed in coculture with unirradiated pneumocytes (17.5 Gy: 30.20% +/- 5.37% [SD]; 0 Gy: 2.77% +/- 4.79%; $P = .002$). Exposure of NIH-3T3 fibroblasts to media conditioned by irradiated, senescent pneumocytes induced radiation dose-dependent increases of fibroblast proliferation (Figure 5G) and soluble collagen production (Figure 5H), effects that were absent when NOX activity in irradiated AECII was inhibited by DPI (mean proliferation of 1.00 +/- 0.08 [SD], 1.67 +/- 0.18, and 1.16 +/- 0.08 for unirradated pneumocyte conditioning, 17.5 Gy, and 17.5 Gy + DPI, respectively, $P < .001$; mean collagen of 132.7 +/- 1.95 [SD], 164.5 +/- 5.47, and 146.9 +/- 9.20 μg/mL for 0 Gy, 17.5 Gy, and 17.5 Gy + DPI, respectively, $P < .001$).

Role of NOX in RIPF

To confirm the importance of NOX in radiation fibrosis, mice were treated with DPI (1mg/kg/day in phosphate-buffered saline) or vehicle control beginning immediately after irradiation (5×6 Gy). Treatment with DPI markedly reduced pulmonary fibrosis after radiation at 16 weeks compared with vehicle (Figure 6A). Similarly, DPI treatment markedly reduced soluble collagen accumulation (5×6 Gy + vehicle: 57.26 μg/lung +/- 11.44 [SD]; 5×6 Gy + DPI: 36.54 μg/lung +/- 4.39; $P = .03$) and hydroxyproline content (5×6 Gy + vehicle: 37.97 μg/lung +/- 5.28 [SD]; 5×6 Gy + DPI: 27.61 μg/lung +/- 5.69; $P = .02$) (Figure 6, B and C).

DHE oxidation was less prevalent in DPI-treated, irradiated lung tissue compared with vehicle-treated, irradiated lung tissue (5×6 Gy + vehicle: 7.62% of cells +/- 2.28% [SD]; 5×6 Gy + DPI: 1.99% +/- 0.64%; $P < .001$)(Figure 6D; Supplementary Figure 5, available online). Furthermore, DPI treatment was sufficient to inhibit radiation-induced AECII senescence (5×6 Gy + vehicle: 37.61% +/- 8.27% [SD]; 5×6 Gy + DPI: 12.38% +/- 4.12; $P < .001$) and AECII depletion (5×6 Gy + vehicle: 1.21 per alveolus +/- 0.17 [SD]; 5×6 Gy + DPI: 1.92 per alveolus +/- 0.17; $P = .01$)(Figure 6, E and F; Supplementary Figure 5, available online).

Discussion

The etiology of RIPF remains controversial (25), but pneumocyte damage has been reported as a major factor in fibrosis of other etiologies. AECII depletion is hypothesized to be a major

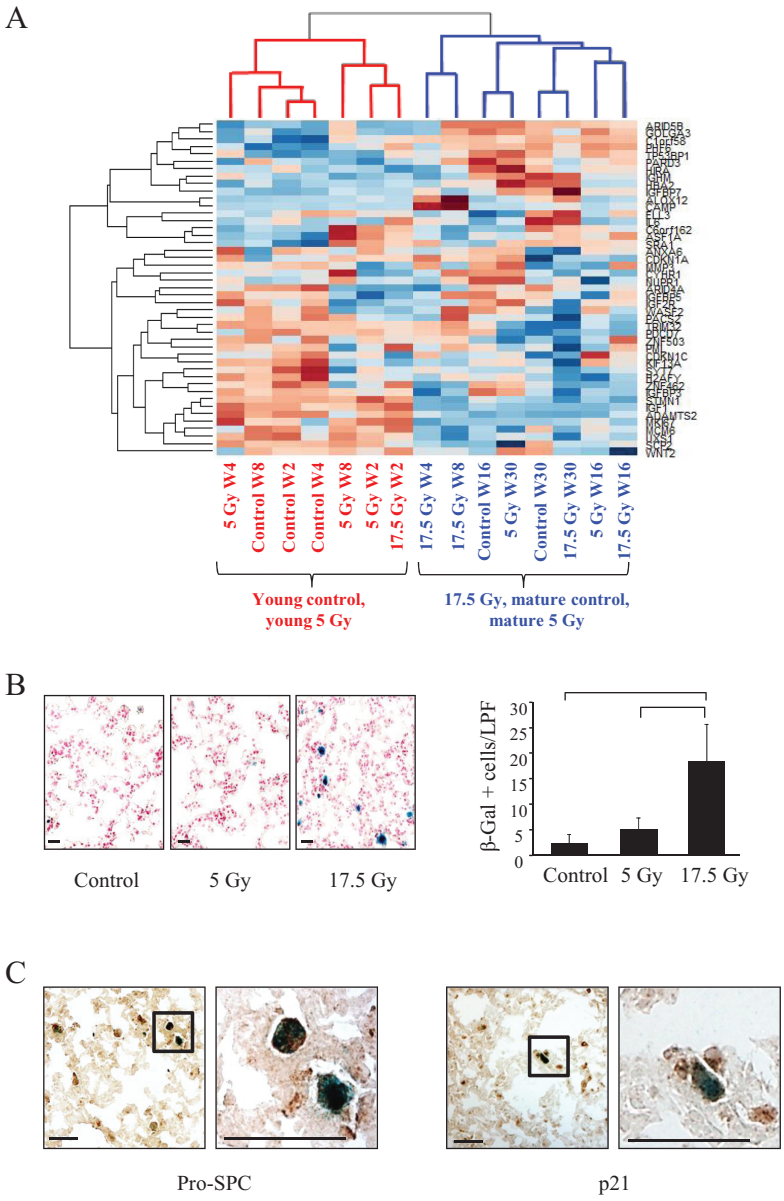

Figure 3. Effects of irradiation (IR) on senescence in mouse lung. C57Bl/6NCr mice were exposed to 0 Gy, 5 Gy, or 17.5 Gy thoracic IR. Samples of lung tissue (n = 3 per condition) were collected at intervals after IR and in control mice. **A**) Hierarchical clustering of samples based on senescence and aging genes. With the exception of the 2-week time point, lung tissue treated to 17.5 Gy clusters with lung from aged, unirradiated mice and aged 5 Gy mice (**blue** color coding). The remainder of the young mice (5 Gy and control) cluster together (**red** color coding). **B**) Representative images of β-galactosidase (β-gal) staining of lung tissue at 4 weeks after IR (**left**) and graphical representation of β-gal–stained cells per 20× field 4 weeks after IR (**right**). Scale bar = 16 μm, low power field (LPF). Bars represent mean. Error bars represent standard deviation. Bracket indicates $P < .05$ by analysis of variance. All statistical tests were two-sided. **C**) Representative low- (**left**) and high-power (**right**) images of costaining for β-gal activity (**blue**) and pro-surfactant C (pro-SPC) (**brown**) or p21 (**brown**) in lung tissue 4 weeks after 17.5 Gy of IR. Scale bar = 16 μm. W = week.

contributor to ineffective alveolar repair (4,26,27), leading to epithelial stress and fibroproliferation (28). Indeed, targeted depletion of AECII resulted in rapidly progressive fibrosis (4). Conversely, delivery of pneumocyte mitogens after radiation restored epithelial integrity and reduced fibrosis at late time points (29).

Loss of pneumocytes has been reported to occur through apoptosis after radiation (8,30). We observed equivalent AECII apoptosis after nonfibrogenic and fibrogenic irradiation, suggesting that AECII apoptosis alone is not sufficient to cause fibrosis. Further, gradual recovery of AECII counts was observed after exposure to 5 Gy but not after exposure to fibrogenic doses. This suggested that regenerative capacity may be dose sensitive and independent of acute cytotoxicity.

Senescence has recently been associated with lung injury. Epithelial senescence has been observed in the lungs of patients with idiopathic pulmonary fibrosis and in animal models of bleomycin-induced pulmonary fibrosis (31,32). Supporting the importance of the replicative potential of pneumocytes in pulmonary fibrosis, mutations of TERT (telomerase reverse transcriptase) and TERC (RNA component of telomerase) have been identified as causes of inherited idiopathic pulmonary fibrosis (33,34).

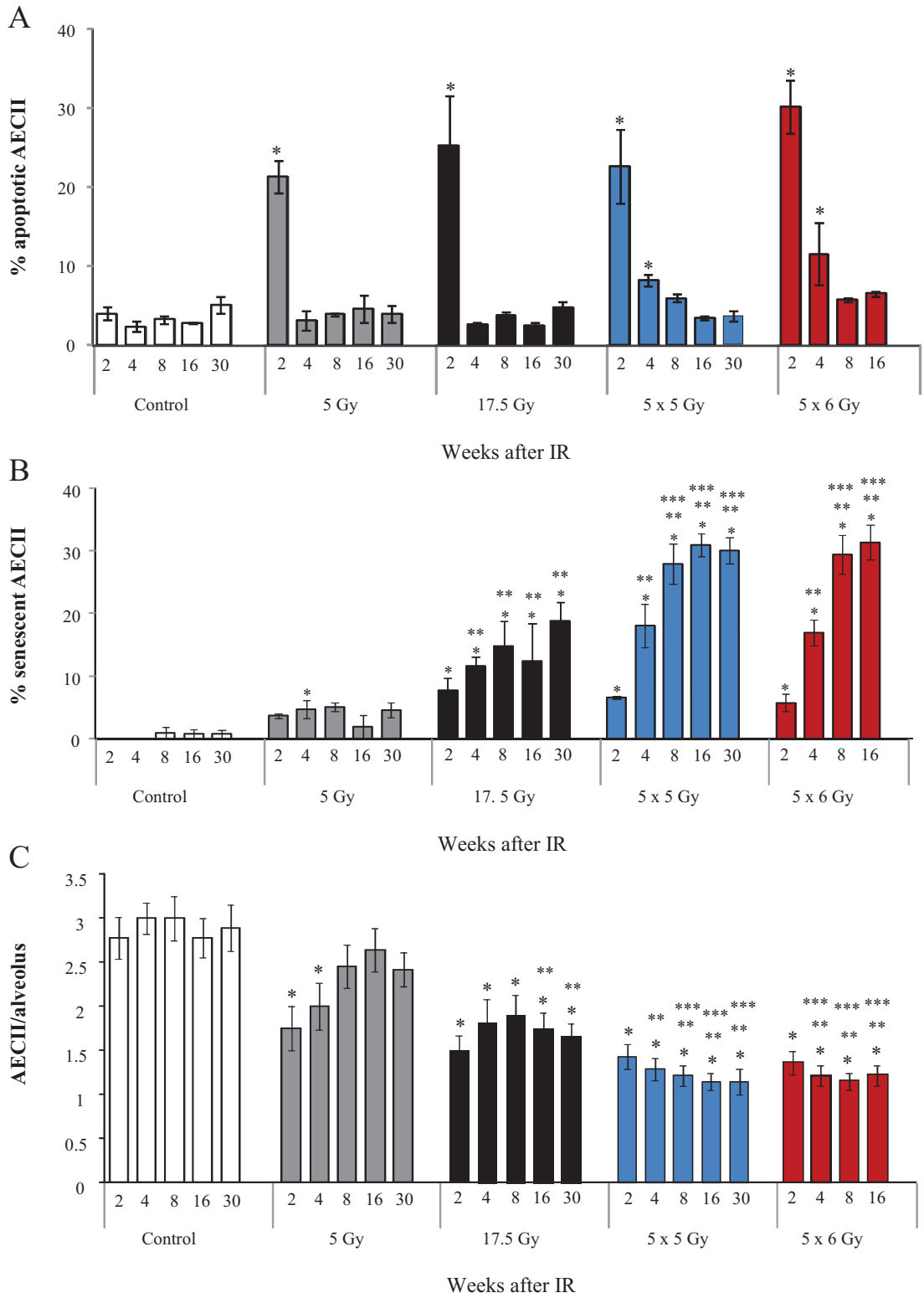

Figure 4. Extent of senescence and apoptosis in irradiated mouse lungs. C57Bl/6NCr mice were exposed to thoracic irradiation at doses of 0 Gy (control), 5 Gy, 17.5 Gy, 5×6 Gy, or 5×5 Gy. Samples of lung tissue were collected at intervals after irradiation (IR) and in controls (n = 3 per dose and time-point). **A**) The percentage of type II airway epithelial cell (AECII) cells that stain for apoptosis (TUNEL) was scored by dose and time point in lungs of mice treated with 0 Gy (control), 5 Gy, 17.5 Gy, 5×5 Gy, or 5×6 Gy. **B**) The percentage of AECII cells that stain for senescence was scored by dose and time point in lungs of mice treated with no IR (control), 5 Gy, 17.5 Gy, 5×6 Gy, and 5×5 Gy. **C**) The number of AECII cells per alveoli was scored by dose and time point in lungs of mice treated with no IR (control), 5 Gy, or 17.5 Gy, 5×5 Gy, and 5×6 Gy. Bars represent the mean. Error bars represent the standard error. $*P < .05$ for the comparison of each treatment to controls; $**P < .05$ for the comparison of irradiated groups to 5 Gy within the same time-point; $***P < .05$ by analysis of variance for the comparison of irradiated groups to 17.5 Gy within the same time point. All statistical tests were two-sided.

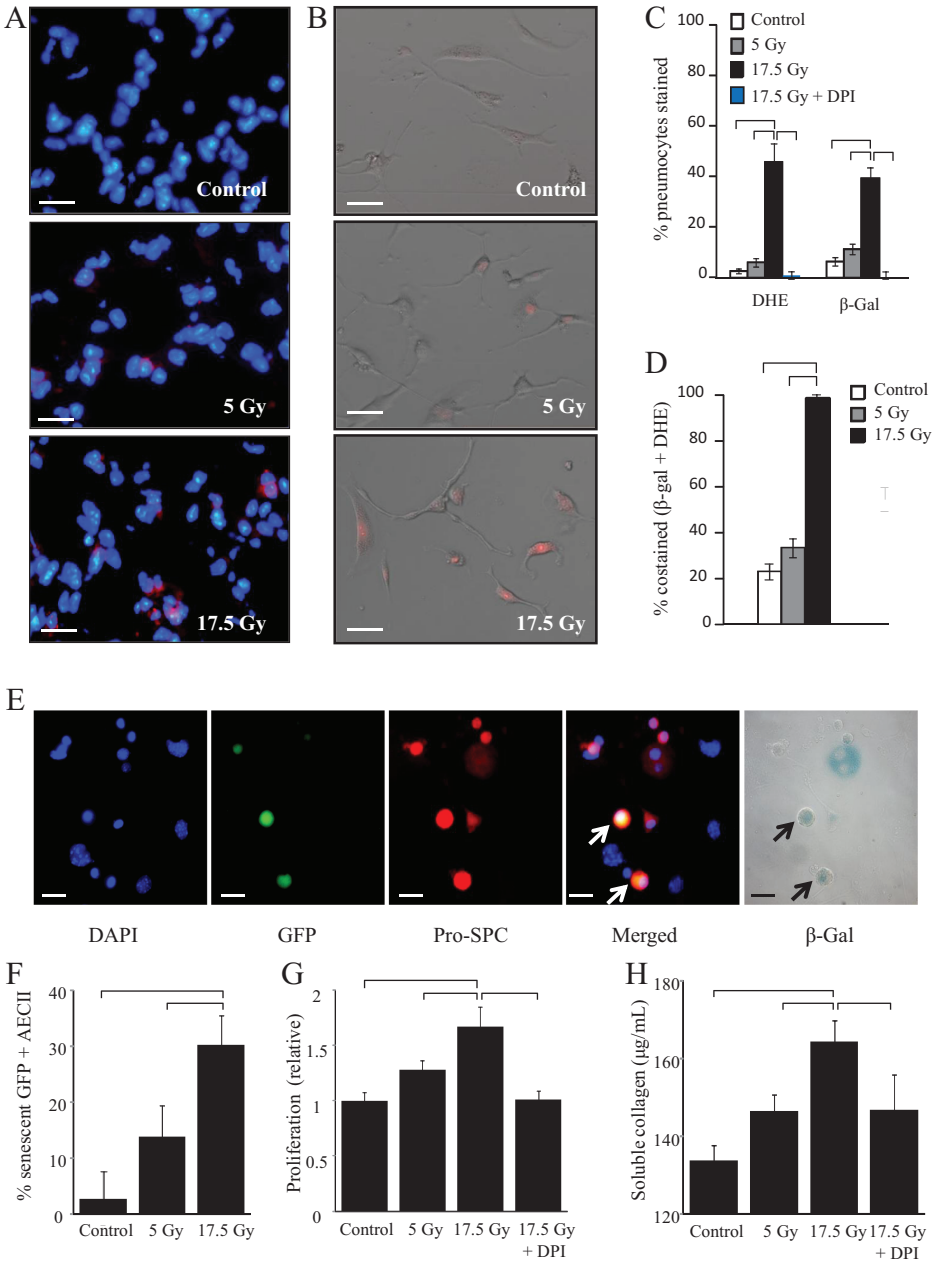

Figure 5. Local and paracrine effects of pneumocyte irradiation (IR). **A**) C57Bl/6NCr mice were exposed to 0 Gy, 5 Gy, or 17.5 Gy thoracic IR (n = 3 per group). At 4 weeks, samples of lung tissue were collected and dihydroethidium (DHE) oxidation was assessed. Scale bars = 16 μm. **B**) Primary pneumocytes were plated and exposed to graded doses of irradiation. DHE oxidation was assessed at 3 days. **C** and **D**) Primary pneumocytes were exposed to 0 Gy (control), 5 Gy, or 17.5 Gy of irradiation and assessed at 3 days. Pneumocytes were treated with diphenyleneiodonium (DPI; 100 nM) immediately before and after IR. DHE oxidation was assessed and cells were costained for β-galactosidase (β-gal) activity. The percentage of pneumocytes staining with DHE and β-gal activity by treatment at 3 days are shown in (**C**). Scale bars = 16 μm. The rate of costaining for β-gal and DHE is shown in (**D**). The low rate of β-gal activity in DPI-treated pneumocytes precluded assessment of colocalization. **E** and **F**) Green fluorescent protein (GFP)-expressing unirradiated primary pneumocytes were cocultured with irradiated primary pneumocytes (17.5 Gy). Cells were fixed after 3 days and costained for β-gal and pro-surfactant C (pro-SPC). **Arrows** in (**E**) point to senescent unirradiated GFP-expressing pneumocytes. Scale bars = 16 μm. The percentage of GFP + type II airway epithelial cells (AECII) staining positive for β-gal activity at 3 days are shown in (**F**). **G** and **H**) Primary pneumocytes were plated and exposed to 0 Gy, 5 Gy, or 17.5 Gy. Conditioned media was collected after 3 days. The effects of treatment with irradiated pneumocyte conditioned media on fibroblast proliferation and collagen production was assessed after 72 hours. Bars represent the mean. Error bars represent the standard deviation. Brackets indicate $P < .05$ by analysis of variance. All statistical tests were two-sided. Scale bar = 40 μm.

Based on microarray data, we hypothesized that AECII depletion resulted from incapacitation of stem cell function by senescence. A time- and dose-dependent increase in AECII senescence and oxidative stress was observed after fibrogenic irradiation. These findings are consistent with the role of AECII as the alveolar stem cell (35), such that loss of replicative potential predisposes to progressive parenchymal depletion and resulting pulmonary fibrosis. Indeed, the degree of senescence, not apoptosis, correlated with the severity of AECII depletion.

Radiation has been described to induce tumor cell senescence (36). Indeed, inducing senescence has been explored as a method to enhance tumor cell killing (17). The data presented here suggest

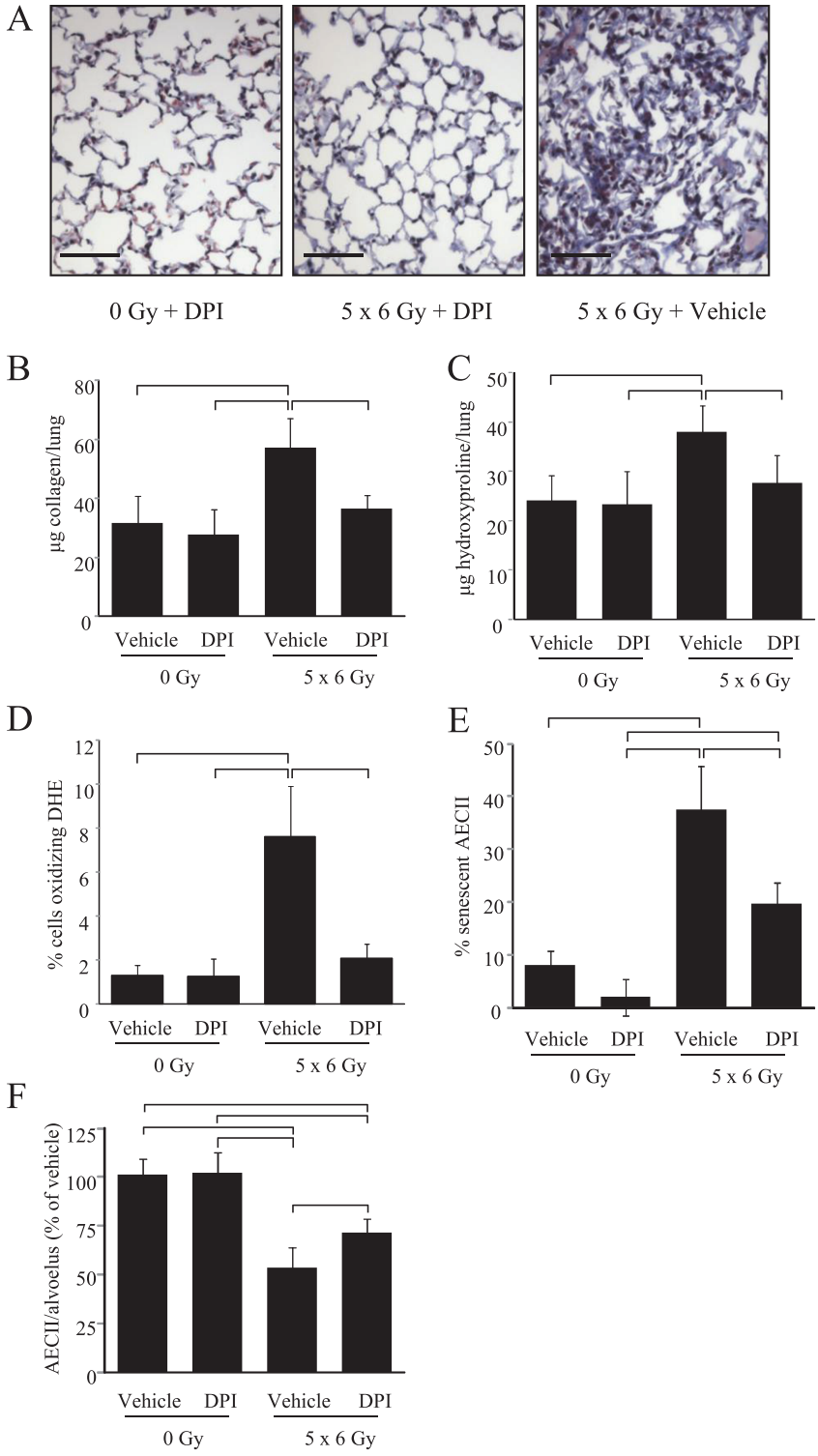

Figure 6. Effect of NADPH oxidase (NOX) inhibition on radiation fibrosis and type II airway epithelial cells (AECII) senescence. C57/Bl6NCr mice (n = 8 per group) were treated with diphenyleneiodonium (DPI; 1 mg/kg in phosphate-buffered saline) or vehicle 5 days per week for 16 weeks, beginning immediately after irradiation (IR) of the thorax to 5×6 Gy or 0 Gy. **A**) Masson trichrome staining of lung tissue collected at 16 weeks after IR (0 Gy or 5×6 Gy). Lungs of mice treated to 5×6 Gy with vehicle develop extensive fibrotic foci, whereas lungs from mice receiving the same radiation dose with DPI develop only minimal collagen deposition. Collagen: **blue**; nuclei: **purple**; cytoplasm/epithelia: **pink**. Collagen content in the R lung at 16 weeks after irradiation was assessed by sircol assay (**B**) and hydroxyproline assay (**C**). Treatment with DPI reduced collagen content after IR compared with vehicle-treated controls. **D**) Frozen sections of lung of mice treated with or without IR and treated with vehicle or DPI were collected at 16 weeks, and dihydroethidium (DHE) oxidation was assessed. **E**) The number of AECII that were senescent was scored in each group at 16 weeks. **F**) The number of AECII per alveolus was scored and is reported as the percentage relative to the vehicle-treated, unirradiated control samples at 16 weeks. Columns represent the mean. Error bars represent the standard deviation. Brackets indicate $P < .05$ by analysis of variance. All statistical tests were two-sided. Scale bar = 40 µm.

that senescence has an important role in normal tissue injury after irradiation. It is possible that the use of agents that enhance senescence with cytotoxic treatments may inadvertently simultaneously enhance radiation toxicity.

Reactive oxygen species are known to induce cellular senescence (37) and are elevated in experimental models of lung injury and fibrosis (9,32,38,39). Superoxide is a potentially toxic reactive oxygen species generated by NOX isoforms. NOX4 has been implicated in epithelial apoptosis after bleomycin exposure (40) and has been described as a source of oxidative stress and apoptosis in irradiated lung (8). We found that inhibition of NOX was sufficient to prevent AECII senescence. Senescent pneumocytes stimulated fibroblast proliferation and collagen secretion, an effect that was blocked with NOX inhibition. These findings suggest that senescent pneumocytes directly stimulate fibrosis by NOX.

Although these data strongly suggest that senescence plays a role in RIPF and that oxidative stress is key in this process, there are limitations in this study. Although these data suggest a role for senescence in RIPF, defining a causative role will require evaluating resistance to fibrosis in mice deficient in senescence. This is a challenging limitation because such mice develop tumors at young ages related to hyperproliferation, precluding the long follow-up required for studying RIPF (41). Perhaps most important, the lack of irradiated human lung tissue for validation is a major limitation of this study. Although the animal models we used are widely used for studies of RIPF, evaluating senescence in human tissues is critical toward understanding the importance of this process in human radiation injury and determining whether these data are applicable to patients. Studying senescence and radiation injury in patients is challenging and limited by lack of frozen tissue from injured sites. The collection of frozen tissue is a high priority to validate these findings. Finally, the importance of senescence in other organs that experience radiation injury was not assessed in this study.

Collectively, these data identify AECII senescence as a novel mechanism of RIPF and NOX as a therapeutic target. Most important, these data suggest that late radiation injury may result from "aging" of tissue by chronic oxidative stress and accelerated stem cell senescence, a finding that could have important implications for patients undergoing radiotherapy.

References

1. Graves PR, Siddiqui F, Anscher MS, Movsas B. Radiation pulmonary toxicity: from mechanisms to management. *Semin Radiat Oncol*. 2010;20(3):201–207.
2. Kapanci Y, Weibel ER, Kaplan HP, Robinson FR. Pathogenesis and reversibility of the pulmonary lesions of oxygen toxicity in monkeys. II. Ultrastructural and morphometric studies. *Lab Invest*. 1969;20(1):101–118.
3. Evans MJ, Cabral LJ, Stephens RJ, Freeman G. Transformation of alveolar type 2 cells to type 1 cells following exposure to NO2. *Exp Mol Pathol*. 1975;22(1):142–150.
4. Sisson TH, Mendez M, Choi K, et al. Targeted injury of type II alveolar epithelial cells induces pulmonary fibrosis. *Am J Respir Crit Care Med*. 2010;181(3):254–263.
5. Osterholzer JJ, Olszewski MA, Murdock BJ, et al. Implicating exudate macrophages and Ly-6C high monocytes in CCR2-dependent lung fibrosis following gene-targeted alveolar Injury. *J Immunol*. 2013;190(7):3447–3457.
6. Almeida C, Nagarajan D, Tian J, et al. The role of alveolar epithelium in radiation-induced lung injury. *PLoS One*. 2013;8(1):e53628.
7. Rube CE, Uthe D, Schmid KW, et al. Dose-dependent induction of transforming growth factor beta (TGF-beta) in the lung tissue of fibrosis-prone mice after thoracic irradiation. *Int J Radiat Oncol Biol Phys*. 2000;47(4):1033–1042.
8. Zhang Y, Zhang X, Rabbani ZN, Jackson IL, Vujaskovic Z. Oxidative stress mediates radiation lung injury by inducing apoptosis. *Int J Radiat Oncol Biol Phys*. 2012;83(2):740–748.
9. Shivshankar P, Brampton C, Miyasato S, Kasper M, Thannickal VJ, Le Saux CJ. Caveolin-1 deficiency protects from pulmonary fibrosis by modulating epithelial cell senescence in mice. *Am J Respir Cell Mol Biol*. 2012;47(1):28–36.
10. Chatterjee P, Choudhary GS, Sharma A, et al. PARP inhibition sensitizes to low dose-rate radiation TMPRSS2-ERG fusion gene-expressing and PTEN-deficient prostate cancer cells. *PLoS One*. 2013;8(4):e60408.
11. Oike T, Ogiwara H, Torikai K, Nakano T, Yokota J, Kohno T. Garcinol, a histone acetyltransferase inhibitor, radiosensitizes cancer cells by inhibiting non-homologous end joining. *Int J Radiat Oncol Biol Phys*. 2012;84(3):815–821.
12. Skinner HD, Sandulache VC, Ow TJ, et al. TP53 disruptive mutations lead to head and neck cancer treatment failure through inhibition of radiation-induced senescence. *Clin Cancer Res*. 2012;18(1):290–300.
13. Kuilman T, Michaloglou C, Vredeveld LC, et al. Oncogene-induced senescence relayed by an interleukin-dependent inflammatory network. *Cell*. 2008;133(6):1019–1031.
14. Coppe JP, Patil CK, Rodier F, et al. Senescence-associated secretory phenotypes reveal cell-nonautonomous functions of oncogenic RAS and the p53 tumor suppressor. *PLoS Biol*. 2008;6(12):2853–2868.
15. Edgar R, Domrachev M, Lash AE. Gene expression omnibus: NCBI gene expression and hybridization array data repository. *Nucleic Acids Res*. 2002;30(1):207–210.
16. RDC T. R: A Language and Environment for Statistical Computing. 2010.
17. Lafferty-Whyte K, Bilsland A, Cairney CJ, et al. Scoring of senescence signalling in multiple human tumour gene expression datasets, identification of a correlation between senescence score and drug toxicity in the NCI60 panel and a pro-inflammatory signature correlating with survival advantage in peritoneal mesothelioma. *BMC Genomics*. 2010;11(532).
18. Zahn JM, Poosala S, Owen AB, et al. AGEMAP: a gene expression database for aging in mice. *PLoS Genet*. 2007;3(11):e201.
19. Herzog EL, Van Arnam J, Hu B, Krause DS. Threshold of lung injury required for the appearance of marrow-derived lung epithelia. *Stem Cells*. 2006;24(8):1986–1992.
20. von Zglinicki T, Saretzki G, Docke W, Lotz C. Mild hyperoxia shortens telomeres and inhibits proliferation of fibroblasts: a model for senescence? *Exp Cell Res*. 1995;220(1):186–193.
21. Chen Q, Ames BN. Senescence-like growth arrest induced by hydrogen peroxide in human diploid fibroblast F65 cells. *Proc Natl Acad Sci U S A*. 1994;91(10):4130–4134.
22. Chen QM, Bartholomew JC, Campisi J, Acosta M, Reagan JD, Ames BN. Molecular analysis of H2O2-induced senescent-like growth arrest in normal human fibroblasts: p53 and Rb control G1 arrest but not cell replication. *Biochem J*. 1998;332(Pt 1):43–50.
23. Chen QM, Liu J, Merrett JB. Apoptosis or senescence-like growth arrest: influence of cell-cycle position, p53, p21 and bax in H2O2 response of normal human fibroblasts. *Biochem J*. 2000;347(Pt 2):543–551.
24. Lu T, Finkel T. Free radicals and senescence. *Exp Cell Res*. 2008;314(9):1918–1922.
25. Trott KR, Herrmann T, Kasper M. Target cells in radiation pneumopathy. *Int J Radiat Oncol Biol Phys*. 2004;58(2):463–469.
26. Kuwano K, Hagimoto N, Kawasaki M, et al. Essential roles of the Fas-Fas ligand pathway in the development of pulmonary fibrosis. *J Clin Invest*. 1999;104(1):13–19.
27. Barbas-Filho JV, Ferreira MA, Sesso A, Kairalla RA, Carvalho CR, Capelozzi VL. Evidence of type II pneumocyte apoptosis in the pathogenesis of idiopathic pulmonary fibrosis (IFP)/usual interstitial pneumonia (UIP). *J Clin Pathol*. 2001;54(2):132–138.

28. Selman M, Pardo A. Role of epithelial cells in idiopathic pulmonary fibrosis: from innocent targets to serial killers. *Proc Am Thorac Soc*. 2006;3(4):364–372.
29. Chen L, Brizel DM, Rabbani ZN, et al. The protective effect of recombinant human keratinocyte growth factor on radiation-induced pulmonary toxicity in rats. *Int J Radiat Oncol Biol Phys*. 2004;60(5):1520–1529.
30. Osterreicher J, Mokry J, Navratil L, et al. The alveolar septal thickness and type II pneumocytes number in irradiated lungs, time expression and the effect of pentoxifylline. *Acta Medica (Hradec Kralove)*. 2001;44(1):15–19.
31. Minagawa S, Araya J, Numata T, et al. Accelerated epithelial cell senescence in IPF and the inhibitory role of SIRT6 in TGF-beta-induced senescence of human bronchial epithelial cells. *Am J Physiol Lung Cell Mol Physiol*. 2011;300(3):L391–L401.
32. Aoshiba K, Tsuji T, Nagai A. Bleomycin induces cellular senescence in alveolar epithelial cells. *Eur Respir J*. 2003;22(3):436–443.
33. Armanios MY, Chen JJ, Cogan JD, et al. Telomerase mutations in families with idiopathic pulmonary fibrosis. *N Engl J Med*. 2007;356(13):1317–1326.
34. Tsakiri KD, Cronkhite JT, Kuan PJ, et al. Adult-onset pulmonary fibrosis caused by mutations in telomerase. *Proc Natl Acad Sci U S A*. 2007;104(18):7552–7557.
35. Reddy R, Buckley S, Doerken M, et al. Isolation of a putative progenitor subpopulation of alveolar epithelial type 2 cells. *Am J Physiol Lung Cell Mol Physiol*. 2004;286(4):L658–L667.
36. Mirzayans R, Scott A, Cameron M, Murray D. Induction of accelerated senescence by gamma radiation in human solid tumor-derived cell lines expressing wild-type TP53. *Radiat Res*. 2005;163(1):53–62.
37. Colavitti R, Finkel T. Reactive oxygen species as mediators of cellular senescence. *IUBMB Life*. 2005;57(4–5):277–281.
38. Zhao W, Diz DI, Robbins ME. Oxidative damage pathways in relation to normal tissue injury. *Br J Radiol*. 2007;80(Spec No 1):S23–S31.
39. Fleckenstein K, Zgonjanin L, Chen L, et al. Temporal onset of hypoxia and oxidative stress after pulmonary irradiation. *Int J Radiat Oncol Biol Phys*. 2007;68(1):196–204.
40. Carnesecchi S, Deffert C, Donati Y, et al. A key role for NOX4 in epithelial cell death during development of lung fibrosis. *Antioxid Redox Signal*. 2011;15(3):607–619.
41. Wolstein JM, Lee DH, Michaud J, Buot V, Stefanchik B, Plotkin MD. INK4a knockout mice exhibit increased fibrosis under normal conditions and in response to unilateral ureteral obstruction. *Am J Physiol Renal Physiol*. 2010;299(6):F1486–F1495.

Funding

All authors were supported by the Intramural Research Program of the National Institutes of Health, National Cancer Institute.

Note

The study sponsor had no role in the design of the study; the collection, analysis, and interpretation of the data; the writing of the manuscript; and the decision to submit the manuscript for publication.

Affiliations of authors: Radiation Oncology Branch (DEC, US, JAH, WS, SZ, HA, AY, EJC) and Radiation Biology Branch (AS, AT), Center for Cancer Research, National Institutes of Health, Bethesda, MD.